AGU PUBLICATIONS

Geophysical Research Letters

RESEARCH LETTER
10.1002/2017GL072524

Key Points:
- The observed relationship between ENSO and the annual cycle over decades cannot be captured by a change to only ENSO or the annual cycle
- In response to forcing from the AMO, the observed changes to ENSO and the annual cycle are consistent with the two being linked
- A coupled model experiment confirms that the AMO impacts ENSO both directly and through changes to the annual cycle

Supporting Information:
- Supporting Information S1

Correspondence to:
A. F. Z. Levine,
aaron.levine@noaa.gov

Citation:
Levine, A. F. Z., M. J. McPhaden, and D. M. W.Frierson (2017), The impact of the AMO on multidecadal ENSO variability, *Geophys. Res. Lett.*, *44*, 3877–3886, doi:10.1002/2017GL072524.

Received 4 JAN 2017
Accepted 11 APR 2017
Accepted article online 17 APR 2017
Published online 30 APR 2017

The impact of the AMO on multidecadal ENSO variability

Aaron F. Z. Levine[1], Michael J. McPhaden[1], and Dargan M. W. Frierson[2]

[1]NOAA/PMEL, Seattle, Washington, USA, [2]Department of Atmospheric Sciences, University of Washington, Seattle, Washington, USA

Abstract Multidecadal shifts in El Niño–Southern Oscillation (ENSO) variability have been observed, but it is unclear if this variability is just a random variation in the ENSO cycle or whether it is forced by other modes of climate variability. Here we show a strong influence of the Atlantic on the multidecadal variability of ENSO. The Atlantic Multidecadal Oscillation (AMO) is the dominant mode of multidecadal sea surface temperature (SST) variability in the Atlantic Ocean. Changes in AMO-related tropical Atlantic SSTs are known to force changes in the Walker circulation in the tropical Pacific Ocean. Using conceptual and coupled model experiments, we show that these changes to the Walker circulation modify ENSO stability on both annual and multidecadal time scales leading to a distinctive pattern of multidecadal ENSO variability that we find in observations and ocean reanalyses.

Plain Language Summary El Niño events have significant global impacts. Over the observed record, periods of both enhanced and reduced El Niño activity exist. The question is whether these changes come purely from random chance or if they are forced from elsewhere in the climate system. Here we will explore the hypothesis that Atlantic multidecadal variability is important for these periods of enhanced and reduce El Niño activity. We will show that the periods of enhanced El Niño activity correspond with periods of increased El Niño predictability and that this signal is consistent with the observed changes in El Niño over the last century and with Atlantic forcing of these changes. The role of the Atlantic sea surface temperature variability will be further confirmed by targeted coupled model experiments.

1. Introduction

Long time series of El Niño–Southern Oscillation (ENSO) show periods of relative quiescence, when the El Niño and La Niña events tend to be weak, and active periods when the El Niño and La Nina events are strong and punctuated with the occasional occurrence of extreme El Niño events [*Wittenberg*, 2009]. The timing of the shifts between periods of active and quiescent ENSO in the recent half century have coincided with changes in the phase of other major multidecadal patterns. This has lead to the hypotheses that the Pacific Decadal Oscillation (PDO) [*Fedorov and Philander*, 2000, 2001] or the Atlantic Multidecadal Oscillation (AMO) [*Dong et al.*, 2006] could influence ENSO on multidecadal time scales. Given the long time scales and the comparatively short record of observations, the relationship between ENSO and other modes of multidecadal variability could just be random [*Wittenberg*, 2009; *Stevenson et al.*, 2012; *Wittenberg et al.*, 2014]. The separation of a possible multidecadal signal from the PDO signal is significantly complicated by the fact that the multidecadal mean state changes could result from averaging over the skewed ENSO system [*Schopf and Burgman*, 2006] and that a substantial fraction of the PDO signal is caused by ENSO [*Di Lorenzo et al.*, 2015].

The first decade and a half of the new millennium have been a relatively quiescent period for ENSO activity, particularly when compared with the previous two decades. Examining these changes in ENSO, *Lübbecke and McPhaden* [2014] found a large increase in stability and decreased growth rate of ENSO anomalies in the latter period compared with the former. Other changes to the tropical Pacific have been observed since 2000, including a cooling of the Pacific cold tongue and an increase in strength of the trade winds [*McPhaden et al.*, 2011]. Hypotheses for these changes in the tropical Pacific mean state include external influences from both the Atlantic [*McGregor et al.*, 2014; *Chikamoto et al.*, 2015] and Indian Ocean SSTs [*Luo et al.*, 2012], as well as internal natural variability. For instance, interbasin SST differences, with the tropical Atlantic warmer than the tropical Pacific, lead to stronger trade winds in the Pacific [*McGregor et al.*, 2014; *Kang et al.*, 2014]. The stronger trade winds impact the mean state of the tropical upper Pacific Ocean leading to changes in the equatorial cold tongue and in thermocline depth and slope [*Kang et al.*, 2014; *Li et al.*, 2015], all of which

affect ENSO stability [*Jin et al.*, 2006; *Lübbecke and McPhaden*, 2014; *Kim and Jin*, 2011]. The effects of increased trade wind strength on the mean state of the tropical Pacific and ENSO stability are consistent with previous modeling studies in which significant fresh water fluxes in the north Atlantic altered the Atlantic Multidecadal Overturning Circulation and the AMO and subsequently found changes in ENSO variance [*Dong et al.*, 2006; *Dong and Sutton*, 2007; *Timmermann et al.*, 2007].

Given that the observational record contains at best two cycles of the AMO, we will not show outright that the AMO impacts ENSO from that record. Instead, we will use a conceptual model of ENSO to demonstrate how a forcing outside of the tropical Pacific must impact ENSO to be consistent with the observed multidecadal ENSO variability. We will then show that in the reanalysis, the ENSO response to the AMO is consistent with the conceptual model prediction. Finally, we will use a coupled climate model experiment to demonstrate the impact of the AMO on ENSO fits with the reanalysis and conceptual model prediction.

2. Data and Methods

2.1. Data

In this study we use Extended Reconstructed Sea Surface Temperature (ERSST) v3b for an extended sea surface temperature reconstruction [*Smith et al.*, 2008]. Monthly SSTs are reconstructed from ICOADS from 1854 to present on a $1^\circ \times 1^\circ$ grid. Simple ocean data assimilation (SODA) 2.2.4 is an extend ocean reanalysis product using the POP ocean model and the NOAA/National Centers for Environmental Prediction Twentieth Century Reconstruction version 2 winds [*Giese and Ray*, 2011]. It provides an estimate of the ocean on a $0.5^\circ \times 0.5^\circ$ grid with 40 vertical levels for the period of 1871–2010. Given the challenges of examining the multidecadal variability in climate reconstructions, we will check our reanalysis results in two independent long single-point time series, the sea level pressure record from Ponta Delgada in the Azores Islands (subtropical Atlantic, and usable as a proxy for the AMO on multidecadal time scales [*Polyakov et al.*, 2010]) and a coral reconstruction from Palmyra Atoll in the central tropical Pacific [*Nurhati et al.*, 2011], which uses both $\delta^{18}O$ and Sr/Ca to reconstruct SSTs at Palmyra Atoll from the 1887 to 1998 with monthly resolution. All of the data have been linearly detrended.

2.2. Methodology

To study the multidecadal variability of ENSO amplitude and ENSO seasonality, we use the spring persistence barrier and the Bjerknes Instability Index. The spring persistence barrier for ENSO comes from the observation that the autocorrelation of ENSO SST anomalies is different depending on the start month with the shortest substantial autocorrelations coming in the boreal spring and the longest in the boreal summer and fall (supporting information Figure S1). The strong tropical Pacific annual cycle determines the seasonal phase locking of ENSO to the boreal winter [*Stein et al.*, 2010; *Dommenget and Yu*, 2016]. The growth rate of ENSO varies throughout the year with a minimum in the boreal spring and a maximum in the boreal fall. These changes in the growth rate lead to what is known as the spring persistence barrier for ENSO, where SST anomalies from the boreal winter have a low correlation with the anomalies in the boreal summer, while SST anomalies in the boreal summer have significant correlations with the SST anomalies in the following boreal winter [*McPhaden*, 2003; *Levine and McPhaden*, 2015]. Changes in the spring persistence barrier can provide important insights into the interaction of ENSO and tropical Pacific annual cycle during this critical time of year for the development of El Niño and La Niña events. Here we will calculate the persistence barrier strength using the autocorrelation of the SST calculated for each month of the year. For each lag τ 1–12, the difference between the maximum and minimum autocorrelation is found. For example, for τ=6, the maximum autocorrelation occurs when the SST starts in August, with $r = 0.85$. The minimum autocorrelation occurs when the SST starts in February, with $r = -0.08$. The difference is 0.93. This difference is then averaged over the lags τ 1–12. The average value over lags 1–12 is determined to be the barrier strength (supporting information Figure S1).

The Bjerknes Instability Index is based on the linear heat budget anomaly derived using a conceptual two-box model for ENSO in the tropical Pacific [*Jin et al.*, 2006]. It assumes that the linear growth rate (λ) can be determined by the changes in the zonal wind, which come from changes in the eastern Pacific SST (μ_a) and drive changes in the zonal currents (β_u), temperature gradients (a_1 and a_2), upwelling (β_w), thermocline slope (β_h), and subsurface temperature anomalies (a_h). The full derivation can be found in *Kim and Jin* [2011].

$$\lambda = -\left(a_1 \frac{\langle \Delta \bar{u} \rangle}{L_x} + a_2 \frac{\langle \Delta \bar{v} \rangle}{L_y}\right) + \alpha_s + \mu_a \beta_u \langle -\frac{\partial \bar{T}}{\partial x} \rangle + \mu_a \beta_w \langle \frac{\partial \bar{T}}{\partial z} \rangle + \mu_a \beta_h \langle \frac{\bar{w}}{H_1} \rangle a_h \quad (1)$$

To study the changes in ENSO amplitude and spring persistence barrier, we use an 11 year running window to smooth the data. Given the strong annual cycle of both the ENSO variance and the ENSO autocorrelation, these time series are also reduced to annual resolution. Eleven year windows prove to be too short to evaluate the changes on the Bjerknes Instability Index on the monthly time scale necessary to resolve the annual cycle in the ENSO growth rate. Therefore, the Bjerknes Instability Index is calculated using a 31 year window. A 31 year window resolves the multidecadal changes to the ENSO amplitude and spring persistence barrier as well but smoothes over the potential Pacific multidecadal impacts (on shorter time scales than the Atlantic), which were examined and found to be weaker correlations than the Atlantic (not shown). Therefore, the results other than the Bjerknes Instability Index remain as 11 year smoothing.

2.3. Coupled Model Experiment

The coupled model is Geophysical Fluid Dynamics Laboratory CM2.1. The atmospheric component has $3.5 \times 3°$ resolution with 24 vertical levels. The oceanic component has nominal 3° ocean resolution increasing to 0.6° latitude resolution at the equator and 28 vertical levels including 5 in the upper 50 m. In the control simulation, the SSTs in the North Atlantic (10°W–80°W, 0–70°N) are relaxed back to the model's monthly climatology with a 2 day relaxation time. In the AMO-forced simulation, the North Atlantic SSTs are relaxed to the monthly climatology plus a 50 year sinusoidally varying AMO anomaly derived by regressing SODA SSTs on the Earth System Research Laboratory AMO index (supporting information Figure S2). Two additional experiments are also run comparing the SST anomalies in separate regions of the AMO forcing. In the tropical (extratropical)-forced AMO experiment, the region of the Atlantic from 0 to 30°N (40°N–70°N) is forced with the 50 year sinusoidal AMO plus seasonal cycle while the rest of the previously prescribed AMO region is relaxed to monthly climatology. Outside of the prescribed regions, the SSTs are allowed to evolve freely. The 50 year time scale from the AMO in these simulations is chosen as a compromise between the period of the decadal variability and computational costs.

3. The Tropical Pacific Annual Cycle and ENSO

To measure the tropical Pacific seasonal cycle changes as they affect ENSO, we develop a method to estimate the strength of the spring persistence barrier of SST and how it varies over time. Previous studies have looked at the relationship between annual cycle amplitude and ENSO using wavelets and spectral transformations, finding an inverse relationship between annual cycle strength and ENSO amplitude [*Gu and Philander*, 1995], although its relevance on long time scales has been questioned [*Emile-Geay et al.*, 2016]. Additional paleoclimate studies have noted that changes in orbital forcing affect the equatorial Pacific mean state during the spring and fall with a subsequent impact on ENSO stability [*Clement et al.*, 1999]. To focus on the annual cycle of ENSO growth rate and in particular the effect of changes in the boreal spring on ENSO, we instead focus on the spring persistence barrier. This has the added benefit of allowing us to also document changes in ENSO predictability [*Levine and McPhaden*, 2015]. When the spring persistence barrier weakens, ENSO is more active (Figure 1). Large El Niño events can happen at any time due to stochastic forcing as evidenced by the outliers in Figure 1, which represent the 1972/1973 and 1997/1998 El Niño events, and single events can significantly impact the periods averages for which they are included [*Schopf and Burgman*, 2006]. Additionally, both the 1972/1973 and 1997/1998 El Niño events have a significant stochastic forcing component that begins during the boreal winter, leading to significant forcing at long lead times. ORA-S4 and the Palmyra coral record are shown in supporting information Figure S3. The Palmyra coral record has the largest correlation between ENSO variance and barrier strength of any of these data sets at $r = -0.7$. These impact of these extreme El Niño events on ENSO variance is likely amplified by the larger temperature anomalies in the eastern Pacific, since the Palmyra coral does not show either the 1972/1973 or 1997/1998 El Niño events as an outlier by this metric. It is also worth noting that the 1982/1983 El Niño event, which is larger than the 1972/1973 event, is not an outlier in any of the data sets.

To better understand what variability is needed to explain these changes, we employ a recharge oscillator conceptual model of ENSO. The version of the recharge oscillator we are using has been previously used to explore the spring persistence barrier [*Levine and McPhaden*, 2015].

$$\frac{\partial T}{\partial t} = -\lambda T + \omega_E h + \sigma\xi(1 + BT) \tag{2}$$

$$\frac{\partial h}{\partial t} = -\omega_E T \tag{3}$$

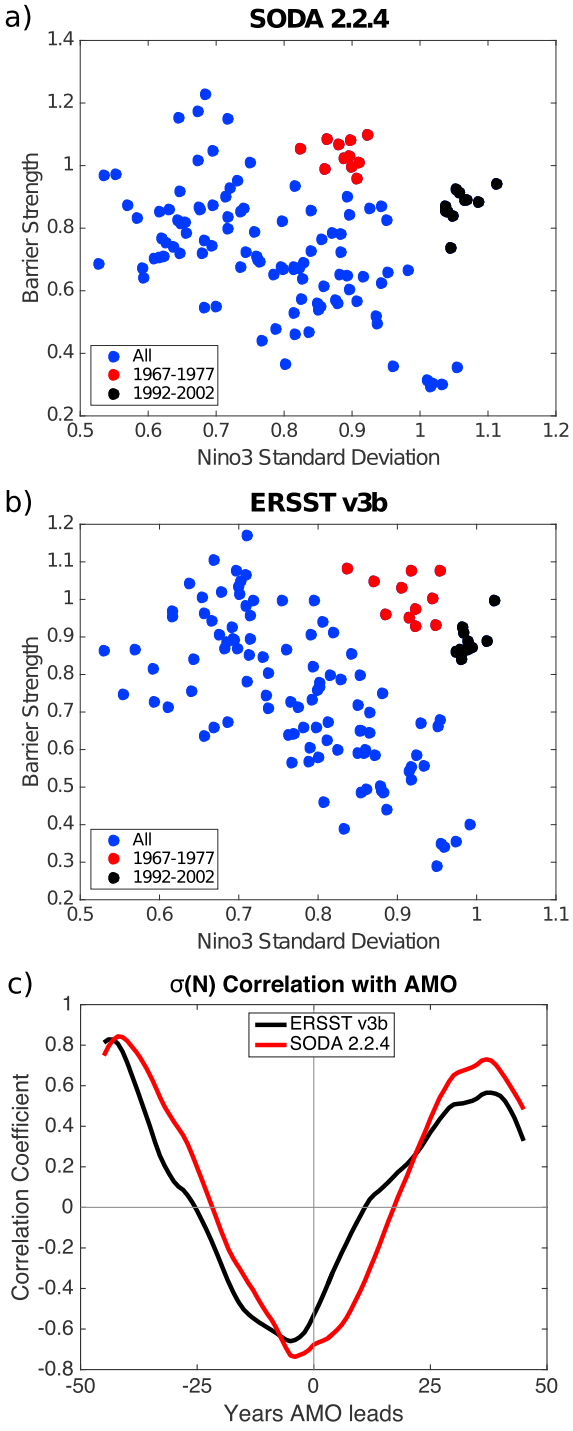

Figure 1. Eleven year running windows show an inverse relationship between the strength of the SPB and ENSO variance both from (a) SODA 2.2.4 which is for the period of 1880–2010 and (b) ERSST v3b from 1880 to 2014. In both data sets, the effect of large El Niño events in 1972 and 1997 are seen for every window that they are included in, which are highlighted by the red and black dots overlaying the original blue points. (c) Correlation of the AMO index with ENSO amplitude ($\sigma(N)$) for the Niño3 index calculated from ERSST v3b and SODA. The AMO leads ENSO amplitude for values on the positive x axis. The time series are smoothed from monthly mean values to annual resolution and have an 11 year sliding window applied.

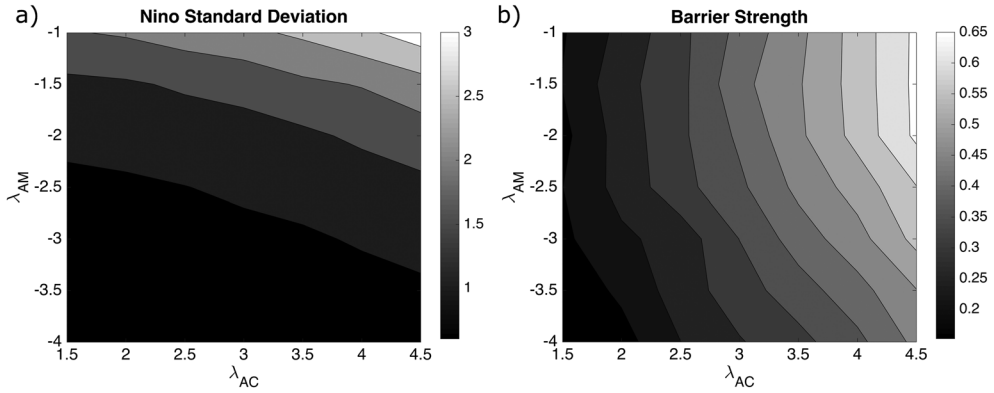

Figure 2. Changes in (a) $\sigma(N)$ and (b) barrier strength in the conceptual model when λ_{am} and λ_{AC} are changed independently of each other. Independent changes of λ_{am} and λ_{AC} do not give the observed inverse relationship between ENSO magnitude and barrier strength.

$$\frac{\partial \xi}{\partial t} = r\xi + w(t) \tag{4}$$

$$\lambda = \lambda_{am} + \lambda_{AC} \sin(\omega_A t) \tag{5}$$

where T is the ENSO state (representing both the SST anomaly and the Bjerknes wind stress response) and h is the heat content anomaly. λ_{am} is the annual mean growth rate and λ_{AC} is the amplitude of the annual cycle of the growth rate. ξ is the Gaussian red noise. The values of the constants $\omega_E = 0.25$, an ENSO period of 4 years, $\sigma = 4.29$, the amplitude of the noise forcing, chosen so that the standard deviation of T is approximately equal to observations, $B = 0.3$, state-dependent noise forcing. To simulate an external forcing, like the hypothesized AMO impact on ENSO, λ_{am} is modified by a sinusoid $\Delta\lambda$ with a period of 50 years. In the case when λ_{AC} is proportional to λ_{am}, the λ_{AC} is determined by equation (6).

$$\lambda_{AC} = \lambda_{AC0} \frac{\lambda_{am}}{\lambda_{am0}} r_{\lambda_{am}\lambda_{AC}} \tag{6}$$

where the initial amplitude of the growth rate annual cycle, $\lambda_{AC0} = 2.5$ and the initial value of the annual mean growth rate, $\lambda_{am0} = 2$, which are the values used in *Levine and McPhaden* [2015]. $r_{\lambda_{am}\lambda_{AC}}$ is the ratio of the change of λ_{AC} each unit change in λ_{am}.

Here we focus on the role of two of the model parameters, λ_{am}, the annual mean growth rate, and λ_{AC}, the annual cycle of the growth rate, as terms mainly responsible for ENSO amplitude and the spring persistence barrier, respectively. Changing either λ_{am} or λ_{AC} independently of the other does not produce the observed relationship between ENSO magnitude and the spring persistence barrier. For constant λ_{am}, increases in λ_{AC} produce an increase in both ENSO amplitude and barrier strength, and for constant λ_{AC}, increases in λ_{am} do not significantly affect barrier strength (Figure 2). However, if λ_{am} and λ_{AC} are inversely related, then the observed relationship between ENSO magnitude and spring persistence barrier emerges for large enough changes in $\Delta\lambda_{am}$ (supporting information Figure S4). Given the uncertainty surrounding the period of the Atlantic multidecadal variability, including whether it is sinusoidal or red noise [*Clement et al.*, 2015], we use the conceptual model to test the sensitivity of $\Delta\lambda$ to period and shape of variability. We find that these changes in $\Delta\lambda$ have a limited impact on the relationship between ENSO amplitude and spring persistence barrier strength when λ_{am} and λ_{AC} are inversely related (supporting information Figure S5). Within the linear framework of the ENSO recharge oscillator, this result leaves two possible hypotheses for the relationship of ENSO magnitude and spring persistence barrier on multidecadal time scales: the null hypothesis that the multidecadal fluctuations of ENSO magnitude and spring persistence barrier are inherent in a stochastically forced, annually phased-locked ENSO [*Stevenson et al.*, 2012; *Wittenberg et al.*, 2014] or, alternatively, as we will show here, that external forcing affects the annual mean ENSO stability and the seasonality of ENSO stability oppositely.

4. The Tropical Atlantic Relationship With ENSO

To first test the hypothesis that the Atlantic SSTs are impacting ENSO stability, we examine the relationship between Atlantic SSTs and ENSO magnitude, defined as the Niño3.4 SST anomaly standard deviation, on an

11 year running window. During the first decade and a half of the new millennium, the AMO became positive and ENSO variance decreased. The AMO and ENSO magnitude from SODA and ERSST v3b are inversely related (Figure 1c). As a check on the reconstructions, we further compare the record from the Palmyra coral and the Azores SLP. The Azores SLP, which is inversely related to and lagged with the AMO [*Polyakov et al.*, 2010] (supporting information Figure S5). The spring persistence barrier and ENSO amplitude measured from the Palmyra coral show the expected relationship with the Azores SLP (supporting information Figure S6). Given that ENSO is known to impact the tropical Atlantic [*Chiang and Sobel*, 2002; *Huang*, 2004], it is worth noting that the effect of El Niño SST anomalies on the Azores SLP is negligible in the year leading and following boreal winter El Niño anomalies (supporting information Figures S7 and S8). Given the statistical challenges of a smoothing and a short record compared with the length of the AMO, these results are not statistically significant at the 95% confidence level. However, we believe that they provide enough evidence to warrant the coupled model simulations that follow.

A positive phase of the AMO is associated with a warming of the SSTs in the north tropical Atlantic. Warmer SSTs in tropical Atlantic lead to a stronger trade winds in the tropical Pacific [*McGregor et al.*, 2014]. The strengthening trade winds have more of an impact on the tropical Pacific mean state during the boreal spring and summer than during other times of year [*Kang et al.*, 2014]. During the boreal spring, the cold tongue disappears, reappearing as the boreal summer progresses. The timing of the disappearance and reappearance of the cold tongue and the upper ocean changes associated with it play an active role in determining the seasonality of ENSO [*Stein et al.*, 2010]. In the next section, we will quantify the effect of this remotely forced seasonal changes in the tropical Pacific on ENSO.

5. Changes in the Tropical Pacific Annual Cycle and Their ENSO Impact

To quantify the impact of the changes in the Atlantic on ENSO, we adopt an approach used in previous studies to estimate both the annual mean stability [*Jin et al.*, 2006; *Kim and Jin*, 2011; *Lübbecke and McPhaden*, 2014] and the seasonality of ENSO stability [*Stein et al.*, 2010] using the Bjerknes Instability Index. The seasonality of ENSO stability comes from the annual cycle in the tropical Pacific. Changes in the cross-equatorial component of the trade winds and the northward migration of the Intertropical Convergence Zone in the boreal summer lead to the seasonal development of the tropical Pacific cold tongue. The seasonal development of the cold tongue and the corresponding annual cycle in zonal temperature gradient, zonal and meridional current, and upwelling all affect the ENSO growth rate. To calculate the multidecadal variability of the annual stability of ENSO growth rate, we calculate the index (We have made a slight modification to the Bjerknes Instability Index. In the original *Kim and Jin* [2011] method, they removed an 84 month running mean from their fields in order to remove the decadal-scale variability. Since examining the decadal-scale variability is our goal, we have omitted that step of the method.) on a 31 year moving window for each month and regress the results on the annual mean AMO index (Figure 3a). Over the course of the year, the damping from the advection of temperature by the mean zonal and meridional currents is both greatly enhanced and greatly reduced in different months. These changes in the mean current structure and evolution have a large impact on ENSO seasonality but a small impact on mean ENSO stability. In contrast, the Ekman feedback, changes in the impact of wind stress-driven equatorial upwelling on ENSO, is more consistent across the months of the year, having a small impact on the seasonality of ENSO but a relatively larger impact on mean ENSO stability. To visualize the differing impacts of the total changes on the seasonality of ENSO and mean ENSO stability, we add the $\pm 2\sigma$ values of the regressed monthly Bjerknes Instability Index to the theoretical seasonal stability from *Stein et al.* [2010] (Figure 3b). The difference in mean stability between periods of the high and low AMO index is $\lambda_{\mathrm{am}} = -0.6\ \mathrm{year}^{-1}$. This result is consistent with the change found between 1980–1999 and 2000–2010 as discussed in *Lübbecke and McPhaden* [2014]. The difference in the seasonality of ENSO stability from high to low AMO index is $\lambda_{\mathrm{AC}} = 0.2\ \mathrm{year}^{-1}$. The ratio of the difference in the mean ENSO stability and the difference in the seasonality of the ENSO stability is within the range estimated from the conceptual model to produce the observed ENSO magnitude and spring persistence barrier relationship. This indicates that the external AMO forcing affects both annual mean ENSO stability and the seasonality of ENSO stability and thus may be responsible for the observed relationship of ENSO magnitude and spring persistence barrier on multidecadal time scales.

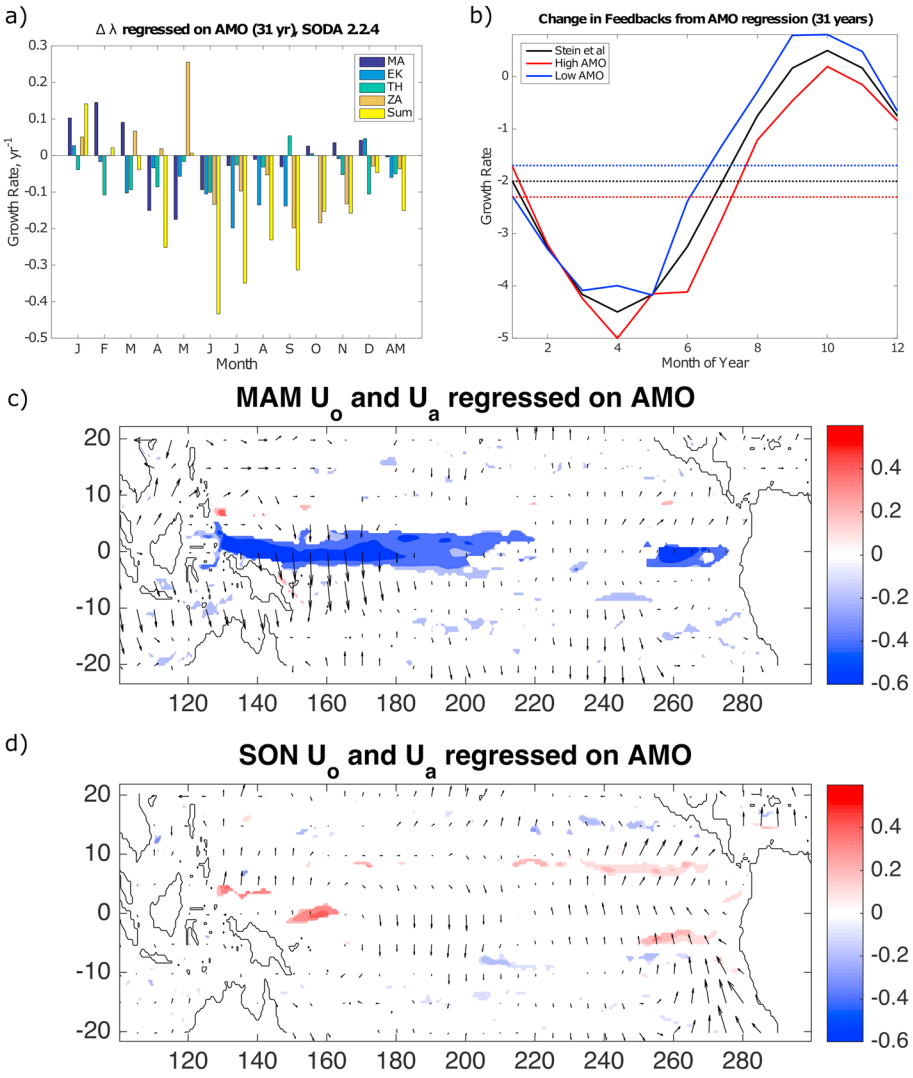

Figure 3. (a) Changes in the Bjerknes Instability index by month regressed on the Azores sea level pressure using 31 year windows with annual resolution. MA is the damping from the advection by the mean current $(-a_1 \frac{\langle \Delta \bar{u} \rangle}{L_x} + a_2 \frac{\langle \Delta \bar{v} \rangle}{L_y})$. EK is the Ekman feedback $(\mu_a \beta_w \langle \frac{\partial \bar{T}}{\partial z} \rangle)$. TH is the thermocline feedback $(\mu_a \beta_h \langle \frac{\bar{w}}{H_1} \rangle a_h)$. ZA is the zonal advective feedback $(\mu_a \beta_u \langle -\frac{\partial \bar{T}}{\partial x} \rangle)$. (b) These feedbacks superimposed on the theoretical ENSO seasonal growth rate from *Stein et al.* [2010]. Different feedbacks have very different seasonal cycles leading to opposite signed changes in λ_{am} and λ_{AC}. Zonal current averaged over 0–50 m (colors, m s^{-1}) and wind stress (arrows, N m^{-2}) from SODA are regressed on the AMO index for the seasons of (e) March–May (MAM) and (f) September–November (SON) showing the changes to the background state that result in seasonal changes to ENSO stability.

6. Pacemaker Experiments

We designed a coupled model experiment to further test the hypothesis that the AMO forces opposite changes in the seasonal and annual mean growth rates of ENSO over multidecadal time periods. In the AMO-forced experiment, the north Atlantic SSTs are relaxed to an AMO SST anomaly pattern (supporting information Figure S2), which varies sinusoidally with a 50 year period. These results are compared with a control simulation where the North Atlantic SSTs are relaxed to the climatological seasonal cycle. The AMO-forced experiment is integrated for 500 years, the tropical-forced and extratropical-forced simulations are integrated for 400 years, and the control simulation is integrated for 100 years. Two additional experiments are performed to examine the respective roles of the tropics and extratropics of the AMO signal on ENSO.

Using the model SST, the relationship between ENSO magnitude and the spring persistence barrier is examined. The control simulation shows no relationship between the two (Figure 4a). In the AMO-forced

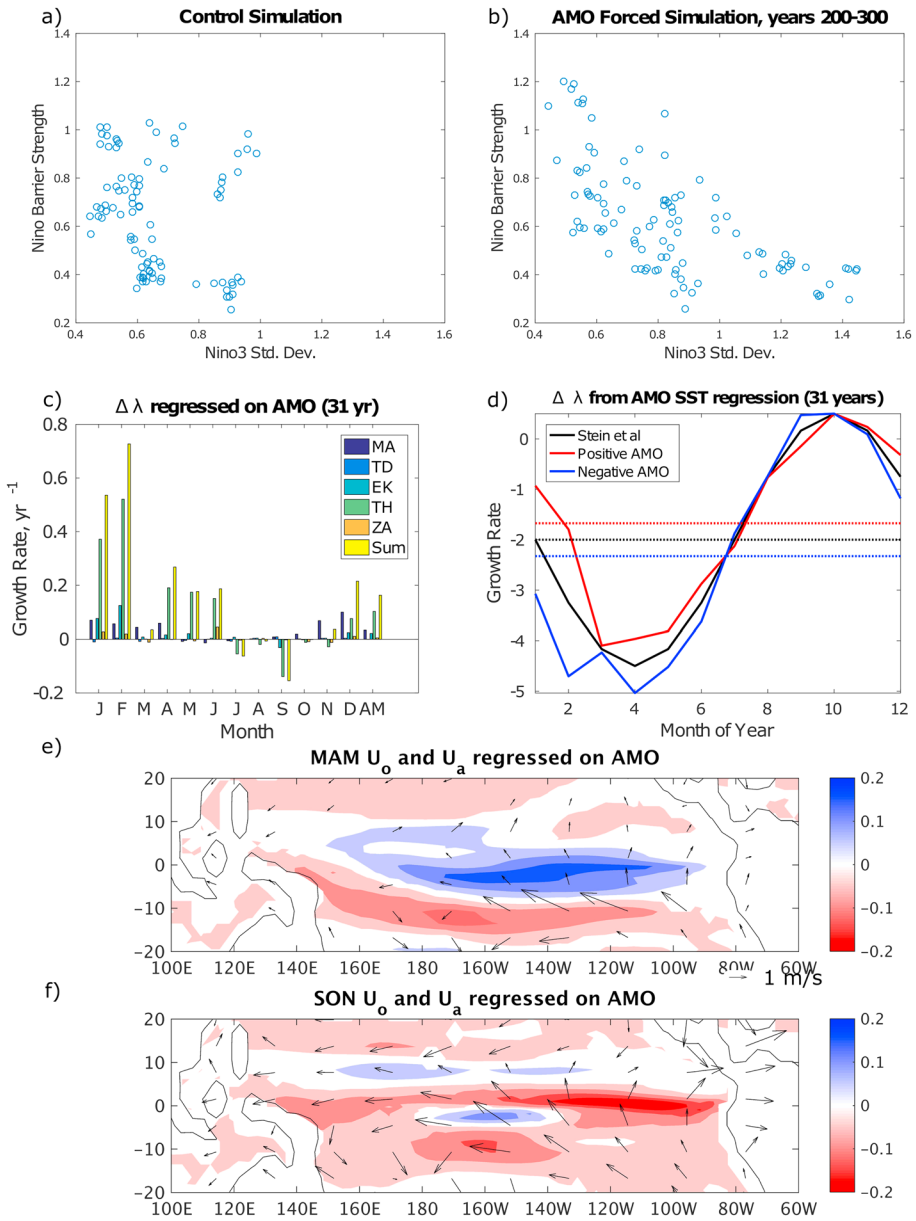

Figure 4. The relationship between the SPB strength and ENSO magnitude in (a) the control simulation and (b) the AMO-forced simulation (100 years shown for clarity). The AMO-forced simulation has an inverse relationship between these two, while the control simulation does not. Using the Bjerknes Instability Index, (c) the monthly feedbacks in the Bjerknes Instability Index are analyzed for the AMO-forced case and (d) superimposed on the theoretical ENSO seasonal growth rate. Like the reanalysis, the different feedbacks have strong monthly signals, which lead to opposite signed changes to λ_{am} and λ_{AC}. Zonal current averaged over 0–50 m (colors) and 1000–850 hPa averaged winds (arrows) (both m s^{-1}) are regressed on the AMO index in the AMO-forced experiment for the seasons of (e) MAM and (f) SON showing the changes to the background state that result in seasonal changes to ENSO stability.

experiment, there is a clear relationship between the ENSO magnitude and the spring persistence barrier strength (Figure 4b). Examining the changes in the Bjerknes Instability Index, the strength of the different feedbacks, particularly the thermocline feedback, varies significantly between different months (Figure 4c). The overwhelming role of the thermocline feedback in the model compared to the reanalysis is due to the previously observed bias in CM2.1 in the thermocline feedback [*Kim and Jin*, 2011], whereby the thermocline flattens too much in response to warming SSTs in the eastern tropical Pacific creating too great of a positive feedback from the thermocline depression onto a developing El Niño event. The large variation from month to month in the thermocline feedback leads to a much smaller change in the annual mean. When the AMO

regressed Bjerknes Instability Index is added to the theoretical ENSO seasonal stability, ENSO during the positive phase of the AMO has an increased annual mean growth rate and a reduced amplitude of the annual cycle of the growth rate (Figure 4d). The variability in the AMO-forced simulation are driven by the changes to the tropical Atlantic; however, the ENSO variability from the North Atlantic simulation is more similar to the observations in large part due to the significant differences in the response of the thermocline feedback to the different forcing regions (supporting information Figure S10). In all of the AMO-forced simulations, the AMO forcing affects both the overall stability of ENSO and the seasonal stability of ENSO, producing the inverse relationship between the ENSO amplitude and the spring persistence barrier on multidecadal time scales.

The AMO affects the tropical Pacific mean state through an atmospheric bridge by altering the trade wind strength in agreement with previous experiments on the influence of Atlantic SSTs on the tropical Pacific [*McGregor et al.*, 2014; *Chikamoto et al.*, 2015; *Kang et al.*, 2014]. During the positive phase of the AMO, SSTs increase in the northern tropical Atlantic. The relatively warmer tropical Atlantic compared with the tropical Pacific strengthens the Walker circulation through an increase in convection in the tropical Atlantic leading to an increase in descending motion and easterly winds over the tropical Pacific [*McGregor et al.*, 2014]. The amount of strengthening of the Walker circulation varies seasonally, with the development of the equatorial cold tongue in the Pacific. Likewise, the changes in cross-equatorial flow and wind stress curl in the tropical Pacific vary between the different seasons. The changes in the wind stress curl significantly affects the equatorial currents in the upper ocean, which plays a large role in the modification of ENSO stability (Figures 3c and 3d, and 4e and 4f) and explain the seasonal variation in the zonal advective feedback and damping from the mean advection in the monthly Bjerknes Instability Index variations (Figures 3a and 4c). The seasonal differences in the changes in tropical Pacific wind stress are consistent with previous studies that have examined the changes in the tropical Pacific on a seasonal time scale [*Kang et al.*, 2014; *Dong et al.*, 2006].

7. Conclusions

In the annual mean, our results agree with *Zanchettin et al.* [2016] that the AMO modifies the thermocline in the tropical Pacific which affects ENSO variance. However, that is only part of the picture for how the AMO modulates ENSO. If the seasonal cycle of ENSO stability remained the same, there would not be a strong relationship between the strength of the spring persistence barrier and ENSO variance. In addition to changes in the annual mean, the AMO also modulates ENSO by changing the seasonal cycle in the tropical Pacific with a positive AMO phase increasing trade wind strength and enhancing the equatorial Pacific cold tongue. Since the cold tongue emerges seasonally, these changes in the seasonal cycle modify the seasonal stability of ENSO, in turn changing the spring persistence barrier. In the most recent decade and a half, following a shift in the AMO to a positive state during the 1990s, these changes have resulted in a period of reduced ENSO activity [*Lübbecke and McPhaden*, 2014] with increased seasonality and decreased predictability 6–9 months before the peak of an El Niño event [*Zhu et al.*, 2015]. Changes to ENSO stability modify the available time for small perturbations in the tropical Pacific SSTs to grow into El Niño events as measured by changes in the spring persistence barrier. Since these changes to the stability in the boreal spring and fall are not equal, the annual mean stability changes as well. These two linked changes are responsible for the simultaneous changes in ENSO predictability and ENSO variance.

Acknowledgments
The authors would like to thank two anonymous reviewers for their helpful suggestions. This research was performed while A.F.Z.L. held a National Research Council Associateship Award at NOAA/PMEL. M.J.M. is supported by NOAA. D.M.W.F. is supported by NSF grants AGS-1359464 and PLR-1341497. This is PMEL contribution 4577. The reanalysis data used in this study are from SODA 2.2.4, which are available at http://apdrc.soest.hawaii.edu/datadoc/soda_pop.php. The AMO index [*Enfield et al.*, 2001] can be downloaded from https://www.esrl.noaa.gov/psd/data/timeseries/AMO/. ERSST v3b is available for download at http://www.ncdc.noaa.gov/data-access/marineocean-data/extended-reconstructed-sea-surface-temperature-ersst-v3b22. The Azores Sea Level Pressure is available from https://crudata.uea.ac.uk/cru/data/nao/nao_azo.dat. The Palmyra coral Sr/Ca-derived SSTs are documented in *Nurhati et al.* [2011] and available for download at ftp://ftp.ncdc.noaa.gov/pub/data/paleo/coral/east_pacific/palmyra2011.txt. Model simulations and MATLAB code available from A.F.Z.L. upon request.

References

Chiang, J. C., and A. H. Sobel (2002), Tropical tropospheric temperature variations caused by ENSO and their influence on the remote tropical climate*, *J. Clim.*, *15*(18), 2616–2631.

Chikamoto, Y., A. Timmermann, J.-J. Luo, T. Mochizuki, M. Kimoto, M. Watanabe, M. Ishii, S.-P. Xie, and F.-F. Jin (2015), Skilful multi-year predictions of tropical trans-basin climate variability, *Nat. Commun.*, *6*, 6869.

Clement, A., K. Bellomo, L. N. Murphy, M. A. Cane, T. Mauritsen, G. Rädel, and B. Stevens (2015), The Atlantic Multidecadal Oscillation without a role for ocean circulation, *Science*, *350*(6258), 320–324.

Clement, A. C., R. Seager, and M. Cane (1999), Orbital controls on the El Niño/Southern Oscillation and the tropical climate, *Paleoceanography*, *14*(4), 441–456.

Di Lorenzo, E., G. Liguori, N. Schneider, J. Furtado, B. Anderson, and M. Alexander (2015), ENSO and meridional modes: A null hypothesis for Pacific climate variability, *Geophys. Res. Lett.*, *42*, 9440–9448, doi:10.1002/2015GL066281.

Dommenget, D., and Y. Yu (2016), The seasonally changing cloud feedbacks contribution to the ENSO seasonal phase-locking, *Clim. Dyn.*, *47*, 3661–3672.

Dong, B., and R. T. Sutton (2007), Enhancement of ENSO variability by a weakened Atlantic thermohaline circulation in a coupled GCM, *J. Clim.*, *20*(19), 4920–4939.

Dong, B., R. T. Sutton, and A. A. Scaife (2006), Multidecadal modulation of El Niño-Southern Oscillation (ENSO) variance by Atlantic Ocean sea surface temperatures, *Geophys. Res. Lett.*, *33*, L08705, doi:10.1029/2006GL025766.

Emile-Geay, J., et al. (2016), Links between tropical Pacific seasonal, interannual and orbital variability during the Holocene, *Nat. Geosci.*, *9*(2), 168–173.
Enfield, D. B., A. M. Mestas-Nuñez, and P. J. Trimble (2001), The Atlantic Multidecadal Oscillation and its relation to rainfall and river flows in the continental U.S., *Geophys. Res. Lett.*, *28*(10), 2077–2080.
Fedorov, A. V., and S. G. Philander (2000), Is El Niño changing?, *Science*, *288*(5473), 1997–2002.
Fedorov, A. V., and S. G. Philander (2001), A stability analysis of tropical ocean–atmosphere interactions: Bridging measurements and theory for El Niño, *J. Clim.*, *14*(14), 3086–3101.
Giese, B. S., and S. Ray (2011), El Niño variability in simple ocean data assimilation (SODA), 1871–2008, *J. Geophys. Res.*, *116*, C02024, doi:10.1029/2010JC006695.
Gu, D., and S. Philander (1995), Secular changes of annual and interannual variability in the tropics during the past century, *J. Clim.*, *8*(4), 864–876.
Huang, B. (2004), Remotely forced variability in the tropical Atlantic Ocean, *Clim. Dyn.*, *23*(2), 133–152.
Jin, F. F., L. L. Pan, and M. Watanabe (2006), Dynamics of synoptic eddy and low-frequency flow feedback. Part I: A dynamic closure, *J. Atmos. Sci.*, *64*, 1677–1694.
Kang, I.-S., H.-h. No, and F. Kucharski (2014), ENSO amplitude modulation associated with the mean SST changes in the tropical central Pacific induced by Atlantic Multidecadal Oscillation, *J. Clim.*, *27*(20), 7911–7920.
Kim, S. T., and F. F. Jin (2011), An ENSO stability analysis. Part II: Results from the twentieth and twenty-first century simulations of the CMIP3 models, *Clim. Dyn.*, *36*(7–8), 1609–1627.
Levine, A. F., and M. J. McPhaden (2015), The annual cycle in ENSO growth rate as a cause of the spring predictability barrier, *Geophys. Res. Lett.*, *42*, 5034–5041, doi:10.1002/2015GL064309.
Li, X., S.-P. Xie, S. T. Gille, and C. Yoo (2015), Atlantic-induced pan-tropical climate change over the past three decades, *Nat. Clim. Change*, *6*, 275–279.
Lübbecke, J. F., and M. J. McPhaden (2014), Assessing the twenty-first-century shift in ENSO variability in terms of the Bjerknes Stability Index, *J. Clim.*, *27*(7), 2577–2587.
Luo, J.-J., W. Sasaki, and Y. Masumoto (2012), Indian Ocean warming modulates Pacific climate change, *Proc. Natl. Acad. Sci. U.S.A.*, *109*(46), 18,701–18,706.
McGregor, S., A. Timmermann, M. F. Stuecker, M. H. England, M. Merrifield, F.-F. Jin, and Y. Chikamoto (2014), Recent Walker circulation strengthening and Pacific cooling amplified by Atlantic warming, *Nat. Clim. Change*, *4*(10), 888–892.
McPhaden, M., T. Lee, and D. McClurg (2011), El Niño and its relationship to changing background conditions in the tropical Pacific Ocean, *Geophys. Res. Lett.*, *38*, L15709, doi:10.1029/2011GL048275.
McPhaden, M. J. (2003), Tropical Pacific Ocean heat content variations and ENSO persistence barriers, *Geophys. Res. Lett.*, *30*(9), 1480, doi:10.1029/2003GL016872.
Nurhati, I. S., K. M. Cobb, and E. Di Lorenzo (2011), Decadal-scale SST and salinity variations in the central tropical Pacific: Signatures of natural and anthropogenic climate change, *J. Clim.*, *24*(13), 3294–3308.
Polyakov, I. V., V. A. Alexeev, U. S. Bhatt, E. I. Polyakova, and X. Zhang (2010), North Atlantic warming: Patterns of long-term trend and multidecadal variability, *Clim. Dyn.*, *34*(2–3), 439–457.
Schopf, P. S., and R. J. Burgman (2006), A simple mechanism for ENSO residuals and asymmetry, *J. Clim.*, *19*(13), 3167–3179.
Smith, T. M., R. W. Reynolds, T. C. Peterson, and J. Lawrimore (2008), Improvements to NOAA's historical merged land-ocean surface temperature analysis (1880–2006), *J. Clim.*, *21*(10), 2283–2296.
Stein, K., N. Schneider, A. Timmermann, and F.-F. Jin (2010), Seasonal synchronization of ENSO events in a linear stochastic model, *J. Clim.*, *23*(21), 5629–5643.
Stevenson, S., B. Fox-Kemper, M. Jochum, R. Neale, C. Deser, and G. Meehl (2012), Will there be a significant change to El Niño in the twenty-first century?, *J. Clim.*, *25*(6), 2129–2145.
Timmermann, A., et al. (2007), The influence of a weakening of the Atlantic Meridional Overturning Circulation on ENSO, *J. Clim.*, *20*(19), 4899–4919.
Wittenberg, A. T. (2009), Are historical records sufficient to constrain ENSO simulations, *Geophys. Res. Lett.*, *36*, L12702, doi:10.1029/2009GL038710.
Wittenberg, A. T., A. Rosati, T. L. Delworth, G. A. Vecchi, and F. Zeng (2014), ENSO modulation: Is it decadally predictable?, *J. Clim.*, *27*(7), 2667–2681.
Zanchettin, D., O. Bothe, H. F. Graf, N.-E. Omrani, A. Rubino, and J. H. Jungclaus (2016), A decadally delayed response of the tropical Pacific to Atlantic Multidecadal Variability, *Geophys. Res. Lett.*, *43*, 784–792, doi:10.1002/2015GL067284.
Zhu, J., A. Kumar, and B. Huang (2015), The relationship between thermocline depth and SST anomalies in the eastern equatorial Pacific: Seasonality and decadal variations, *Geophys. Res. Lett.*, *42*, 4507–4515, doi:10.1002/2015GL064220.